Atmos. Chem. Phys. Discuss., doi:10.5194/acp-2016-876, 2016
Manuscript under review for journal Atmos. Chem. Phys.
Published: 14 November 2016

Atmospheric Chemistry and Physics
Discussions

Large-scale atmospheric circulation control on stable water isotopes in precipitation over the northwestern and southeastern Tibetan Plateau

Xiaoxin Yang*[1,2], Sunil Acharya[1,3], Tandong Yao[1,2]

1. Laboratory of Tibetan Environment Changes and Land Surface Processes , Institute of Tibetan Plateau Research, Chinese Academy of Sciences, No. 16 Lincui Rd., Chaoyang District, Beijing 100101, China

2. CAS Center for Excellence in Tibetan Plateau Earth Sciences, Beijing 100101, China

3. University of Chinese Academy of Sciences

Correspondence: X. Yang, email: xxy@itpcas .ac.cn

Abstract

The mid-latitude westerlies and South Asian Summer Monsoon (SASM) are two major atmospheric circulation systems influencing the Tibetan Plateau (TP). We report a seven-year (2007/2008-2013/2014) dataset of $\delta^{18}O$ in precipitation ($\delta^{18}O_p$) collected at three stations. Taxkorgan (TX) and Bulunkou (BLK) are located on the northwestern TP where westerly winds dominate while Lulang (LL) is situated on the southeastern TP where the SASM dominates. $\delta^{18}O$ in precipitation ($\delta^{18}O_p$) in northwestern TP varies with surface temperature (T) throughout the study period, and is depleted in ^{18}O in precipitation during June to September when the monsoonal circulation enters the TP. Integration with model outputs suggests that large-scale atmospheric circulation plays a major role in isotopic seasonality in both regions. A teleconnection between precipitation on the northwestern TP and the El Niño-Southern Oscillation (ENSO) warm phase is suggested by changes in the relationship between $\delta^{18}O$ and δD (e.g., reduced slope and weighted d-excess) in precipitation samples. These observations are indicative of a weakening of the mid-latitude westerly jet allowing local processes in the continental interior to become more dominant, thereby increasing the contribution of secondary evaporation from falling raindrops and kinetic fractionation. Under the conditions of a high Northern Annular Mode (NAM) the westerly jet is intensified over the southeastern TP which enhances local

Atmos. Chem. Phys. Discuss., doi:10.5194/acp-2016-876, 2016
Manuscript under review for journal Atmos. Chem. Phys.
Published: 14 November 2016

evaporation and continental recycling as revealed by a lower δD- $\delta^{18}O$ slope and intercept, but higher d-excess average in contemporaneously collected precipitation samples. The significant correlation between T and $\delta^{18}O_p$ in the northwestern TP during various composite periods highlights a variation from 0.39‰/℃ (ENSO warm) to 0.77‰/℃ (high NAM), attributable to decreased (increased) water vapor availability over the northwestern TP during the ENSO warm (strong positive NAM) phase. ENSO cold and strong negative NAM phases show analogous effects on atmospheric circulation over both regions.

Keywords

stable water isotopes; precipitation; Tibetan Plateau; large-scale atmospheric circulation; westerly; summer monsoon; El Niño-Southern Oscillation; Northern Annular Mode

1 Introduction

The Tibetan Plateau (TP) contains the largest mass of ice outside the Arctic and Antarctica, and serves as a Water Tower to East Asia (Immerzeel and Bierkens, 2010). With ice core records revealing high-resolution paleoclimate information in the tropical and sub-tropical alpine regions, it also stores a unique natural archive of Earth's climate history (Thompson et al., 2011). Under global warming, however, climate and environment on the TP is undergoing dramatic changes. Cryospheric changes are very prominent and lead to hydrological changes and modify the atmospheric circulation and land-surface processes in mid-latitudes and the Northern Hemisphere (Allen and Zender, 2011;Bamzai and Shukla, 1999;Lu et al., 2008;Xu et al., 2009;Bolch et al., 2012;Gardner et al., 2013;Yao et al., 2012). Recent research reveals heteorogeneous variation of glacial mass balance over the TP with accelerated retreating on the southern TP and more stable (or in some cases advancing) glaciers on the northwestern TP (Bolch et al., 2012;Gardner et al., 2013;Yao et al., 2012). Some studies attribute this heterogeneity to precipitation(Fujita, 2008), or to spatially different temperature variations (Gardner et al., 2013), while others attributed this to changes in the atmospheric circulation characterized by a weakening summer monsoon and enhanced westerly flow (Yao et al., 2012).

Many uncertainties exist with regard to range of the influence and interactions among various atmospheric circulation regimes over the region (An et al., 2012;Conroy and Overpeck, 2011;Rozanski et al., 1992). Using the spatial pattern of stable isotopes in precipitation, Yao and his colleagues (2013) proposed regions north of 35°N on the TP as the westerly domain, where most of the moisture originates from the Atlantic, Mediterranean and Caspian Sea, as well as continental recycling throughout the year (Aizen et al., 2006), while the monsoon domain south of 30°N on the TP is dominated by the South Asian Summer monsoon (SASM) circulation. Recent studies bring new insights to this highly generalized view. For example, the decadal (2001-2011) variation of the mass balance of Zhadang glacier (30 °N) on the southern TP is strongly impacted by mid-latitude westerlies Additionally, tropical forcing has been linked to higher latitude climate changes in the Northern Hemisphere (Ding et al., 2014;Zhao et al., 2014). Better qualification of the interactions between the westerlies and SASM is important to understand climate and environmental changes on the TP, not only for the current global change scenario (Zanchettin et al., 2008), but also for long-term climate fluctuation over geological timescales (An et al., 2012).

The details of the interactions between the westerlies and the SASM remain a topic of investigation within the atmospheric community (e.g.,Chiang et al., 2015; Liu and Yin, 2001; Park et al., 2012; Sugimoto and Ueno, 2010). One prominent view is that westerly winds dominate over the TP until the early monsoon season (April-June), but almost disappear during the monsoon mature phase (Park et al., 2012). This led to the scenario of retreating westerlies and intrusion of the SASM (Park et al., 2012). While another study (Liu and Yin, 2001) has proposed an in-phase variation of the westerlies with the SASM such that intensified westerlies between 40° N and 50° N associated with a strengthening (more positive) North Atlantic Oscillation (NAO) would reinforce the bifurcating flows to the south and southeast of the TP, thus generating cyclonic flow over the eastern TP. Moreover, a study of the latent heat field on the TP suggests a possible weakening of the intrusion of marine moisture from the Bay of Bengal (BOB) in association with the weakening of subtropical westerlies (Sugimoto and Ueno, 2010). General circulation models help illuminate the complex interactions between the two dominant circulation regimes over the TP. Yet modeling studies also require verification and refinement that depends upon utilization of such ground observations include stable water isotopes in precipitation ($\delta^{18}O_p$) that contribute to tracing moisture sources and unraveling atmospheric circulation patterns (Araguas-Araguas et al., 2000;Froehlich et al., 2008;Kendall and Caldwell, 1998;Pearson et al., 1991;Rozanski et al., 1992;Tian et al., 2007;Vuille et al., 2005).

Data collected by the Global Network of Isotopes in Precipitation (GNIP) provides a map of the climatological oxygen isotopic composition of precipitation for January (representative of winter) and July (summer) over the Eurasian continent (Fig.1). The maps reveal seasonally distinct distributions of $\delta^{18}O_p$ in the TP region, i.e., lower (more depleted in ^{18}O) in winter and higher (more enriched in ^{18}O) in summer over the northwestern TP relative to that over the southeastern TP. The corresponding atmospheric circulation reveals a close link between the wind circulation and the temporal and spatial variability of $\delta^{18}O_p$ (Fig. 1). The dominance of westerly flow during January contributes to spatial features reflecting the latitudinal temperature distribution, while the dominance of the SASM during July leads to isotopic depletion in the southeastern TP with deep monsoon convection. Thus large-scale atmospheric circulation appears to be an important control on the spatial distribution of $\delta^{18}O$ on the TP. Under anticipated global changes, the atmospheric circulation over the TP is expected to change due to expected variations in surface processes (snow cover, vegetation, permafrost variation), and modulation of the sea surface temperatures (Wu and Zhang, 1998;Ye and Wu, 1998;Zhao et al., 2007;Sugimoto and Ueno, 2010). Understanding how stable isotopes in precipitation respond to such changes will better elucidate the teleconnection between the large-scale atmospheric circulation regimes and water vapor transport over the TP. Additionally, the use of paleoproxies such as ice cores, lake sediment, tree rings and speleothem should facilitate the identification of extreme climatic phases in the historical record (Rowley and Garzione, 2007).

This research uses $\delta^{18}O_p$ as a bridge to link local processes with large-scale atmospheric circulations, and thereby better elucidate the interactions between large-scale atmospheric circulation regimes and local climate changes in the southeastern and northwestern TP. In many tropical regions year-to-year monsoonal variations are affected by El Nino-Southern Oscillation (ENSO) (IPCC, 2013). And the westerly jets are closely related to the evolution of the Northern Annular Mode (NAM). So this study focuses on the southeastern and northwestern parts of the TP to present for the first time the stable isotopic composition in precipitation (including $\delta^{18}O_p$ and δD) of 7-year continuous time series, aiming to evaluate possible effects of large-scale atmospheric circulation such as ENSO and NAM on moisture sources and atmospheric circulations over the southeastern and northwestern regions. This study also presents a brief comparison of our field observations with available model outputs, to quantify contributions of different moisture sources to local precipitation in different areas on the TP, and to verify different roles of local recycling versus large-scale atmospheric circulations in $\delta^{18}O$ variations. The unique dataset will enable the consideration of climate changes over the TP against the large-scale atmospheric circulation scenario, and thus contribute to ground validation of general circulation models equipped with stable isotopes.

2 Sampling and data processing

To investigate possible monsoon-westerlies interactions, this study reports a seven-year record (2007/2008 to 2013/2014) at three stations, Lulang (LL; 29º46′N, 94º44′E, 3330 m above sea level (m a.s.l.)) on the southeastern TP, and Taxkorgan (TX; 37º46′N, 75º16′E, 3100 m a.s.l.) and Bulunkou (BLK; 38º39′N, 74º58′E, 3306 m a.s.l.) on the northwestern TP (Fig. 2). A previous study confirmed the BOB summer monsoon dominance over LL (Yang et al., 2012). The two northwestern TP stations are located in the mid-latitudes, where the westerly jet prevails throughout the year. The local meteorological stations at these three sites collected precipitation for subsequent isotopic analyses. The stations are equipped with a refrigerator and manned by staff who are trained observers and required to be on duty-shifts covering 24 hours per day. Event-based precipitation amounts exceeding 0.1 mm is first collected in a deep bucket, and then immediately poured in a 15 ml polyethylene bottle, appropriately marked, sealed tightly and refrigerated until measurement. For snow sampling, snow is first collected in a plastic bag placed in the bucket, and then brought indoors to melt before being poured into the bottle which is also labeled and stored. Simultaneous meteorological parameters that are recorded include air temperature (T), precipitation amount (P), relative humidity (RH), wind speed, and the start/finish of the event. Precipitation samples were assembled roughly every ten months and returned for measurement at the Chinese Academy of Sciences Key Laboratory of Tibetan Environmental Changes and Land Surface Processes. Stable isotopic composition in precipitation ($\delta^{18}O_p$ and δD_p) samples were measured on a Picarro-L1102i of Picarro Inc., Santa Clara, California, using wavelength scanned cavity ring down spectroscopy (WS-CRDS) with a precision for $\delta^{18}O_p$ of 0.1‰ and for δD_p of 0.5‰. For days experiencing more than one event, the daily amount-weighted means of the δ values is presented.

Temperature discussed in this paper is precipitation-synchronous local temperature, which is slightly different from the daily averages. Because the composition of stable isotopes in precipitation is directly influenced by the temperature during precipitation formation, the temperatures presented in the study are more relevant for the interpretation. We refer to the quality control criteria for event precipitation sampling at Nur (Dec., 1990- October, 1992) in the GNIP dataset (www-naweb.iaea.org), where records with the absolute d-excess ($d = \delta D - 8\times\delta^{18}O$) values >40 are considered to be extreme. We applied this same quality control criterion to our data and removed the extreme values from the further analysis. The processes creating such extreme values warrant future investigation but are beyond the scope of this paper.

To investigate atmospheric circulation interactions , ERA-interim reanalysis data at a spatial resolution of $0.75^{\circ}\times0.75^{\circ}$ are acquired from the ECMWF Public Datasets, including monthly meridional and zonal wind, specific humidity at 37 pressure levels, and vertically integrated water vapor flux and divergence. Globally-complete fields of monthly Sea Surface Temperatures (SSTs) on a $1^{\circ}\times1^{\circ}$ grid are obtained from the Met Office Hadley Centre's sea ice and sea surface temperature (HadISST) data set(Rayner et al., 2003). Daily Arctic Oscillation (AO) and North Atlantic oscillation (NAO) indices are acquired from the National Oceanic and Atmospheric Administration (NOAA) Climate Prediction Center (CPC). Both circulation systems are considered leading teleconnection patterns in the Northern Hemisphere. Monthly and annual NAO and AO data are retrieved from htTP://climatedataguide.ucar.edu/climate-data/hurrell-north-atlantic-oscillation-NAO-index-station-bas

Atmos. Chem. Phys. Discuss., doi:10.5194/acp-2016-876, 2016
Manuscript under review for journal Atmos. Chem. Phys.
Published: 14 November 2016

ed. Monthly SST data and their anomalies (base period: 1981-2010) in different Nino regions from January 1950 to the present are acquired from ERSST Version 4.0 at www.cpc.ncep.noaa.gov .

3 Results

3.1 Variation of $\delta^{18}O_p$

Precipitation days at TX totaled 231 during 2008-2014, with the most occurrences in 2008 and the least in 2011 (Table 1). According to the China Meteorological Administration database, annual precipitation amount averages around 109 mm during the period, varying from 58.9 mm in 2009 to 117.4 mm in 2010, and surface temperature averages 7.7℃ on precipitation days. Mean temperatures on all precipitation days vary widely from year to year. For example, in 2008 the mean daily temperature was 3.2℃ when over 30% of annual precipitation fell as snow, while in 2012 of similar precipitation frequency, the mean temperature was 10.3℃ when only 8% of annual precipitation fell as snow (Table 1). Daily $\delta^{18}O_p$ exhibits the smallest (largest) range and variance in 2009 (2008).Concerning inter-annual variability, the highest annual amount-weighted average value (.8‰) occurred in 2009 and the lowest value (-11.0‰) in 2011. The most enriched $\delta^{18}O_p$ values all occur during July-August, while the most depleted values are irregularly distributed throughout the year (Fig. 3a).

Table 1 Basic information of sampling stations reported in this study.

			$\delta^{18}O$ (‰)			T	Precipitation days
ID	Period covered		Min	Max	Mean	(℃)	total
TX	2008.1~ 2014.10	2008	-27.0	12.2	-6.6	3.2	49
TX		2009	-8.4	11.6	-0.1	7.9	19
TX		2010	-20.7	3. 3	-8.1	9.9	35
TX		2011	-25.3	5.3	-11.0	10.4	14
TX		2012	-26.2	5.8	-6.8	10.3	48
TX		2013	-17.4	9.9	-7.7	8.3	34
TX		2014	-19.1	6.8	0.8	11.8	32
BLK	2008.1~ 2014.11	2008	-22.3	2.6	-6.6	4.6	31
BLK		2009	-18.2	4.3	-7.3	3.4	31
BLK		2010	-28.8	0.1	-11.1	4.6	86
BLK		2011	-28.6	1.4	-12.5	0.3	44
BLK		2012	-26.0	1.1	-8.3	1.4	49
BLK		2013	-24.2	-2.3	-11.6	-0.2	56
BLK		2014	-25.1	3.3	-12.2	5.3	66
LL	2007.1~ 2013.12	2007	-27.8	0.9	-16.0	7.8	119
LL		2008	-28.3	1.8	-14.0	8.1	141
LL		2009	-19.0	3.5	-10.6	8.0	104
LL		2010	-24.0	0.0	-13.0	7.5	121

Atmos. Chem. Phys. Discuss., doi:10.5194/acp-2016-876, 2016
Manuscript under review for journal Atmos. Chem. Phys.
Published: 14 November 2016

LL	2011	-20.9	3.5	-12.8	9.2	53
LL	2012	-25.7	3.2	-13.5	8.0	85
LL	2013	-22.6	0.6	-13.1	6.3	88

$\delta^{18}O_p$ at BLK is generally more depleted than that at TX, with the lowest values occurring during November-March, while the highest values occur irregularly over the year (Fig. 3b). The most precipitation days (86 days) were observed in 2010 while the least precipitation days (31 days) occurred in 2008 and 2009. The lowest value of the annually amount weighted $\delta^{18}O_p$ occurred in 2011, and the highest value occurred in 2008. Similar to TX, monthly $\delta^{18}O_p$ at BLK varies closely with temperature (Fig. 3b).

Precipitation is more frequent at LL than the two stations in northwestern TP. About 36% of all precipitation days experienced daily amounts surpassing the daily average. Most precipitation during November-February (i.e., winter) falls as snow, with 2009 showing 36% of all snowy days during the seven-year period. The most enriched daily $\delta^{18}O_p$ during the study period occurred in spring (April-May), and the most depleted values appear in spring (March-May) (Fig. 3c). $\delta^{18}O_p$ at LL demonstrates the most depleted annual weighted average (-16.0‰) in 2007 while the most enriched one (-10.6‰) in 2009, with Year 2008 in between witnessing the largest variation range of daily $\delta^{18}O_p$ during the 7-year period.

The 7-year monthly averages show clear seasonality of monthly temperature, precipitation amount and amount-weighted $\delta^{18}O_p$. Precipitation amount during summer (June-September) is high in both the southeastern and northwestern TP, with seasonal precipitation amount taking up ~83.5% at BLK, 61.3% at LL, and ~44.3% at TX of the annual total. Amount-weighted $\delta^{18}O_p$ at both TX and BLK shows high values with summer warmth during June-September and low values in other months (Fig. 3d, e), while that at LL shows dramatic depletion at high temperature and precipitation amount during summer (Fig. 3f), thus demonstrating remarkable inter-station and intra-seasonal differences.

3.2 variation of d excess

Deuterium-excess (d) is calculated as $d=\delta D-8\times\delta^{18}O$. It is indicative of moisture sources and transport processes (Froehlich et al., 2008), and is closely affected by moisture source humidity, wind speed and sea surface temperature(Clark and Fritz, 1997). The monthly d-excess at the northwestern TP stations has much larger amplitude than that at the southeastern TP station (Fig. 4). In the northwestern TP, d excesses are generally high during June-September, while low during January-April (Fig. 4a, b).

This is consistent with temperature variation in the northern hemisphere. In comparison, a noticeable decrease of *d*-excess values is observed at LL during June-September (Fig. 4c), when both temperature and precipitation amount are high, indicating humidity increases over the BOB with the monsoon evolution in summer.

3.3 Seasonal variation of isotopes in precipitation

Daily $\delta^{18}O_p$ shows a strong linear correlation with δD_p at all three stations, though with distinct seasonality for each station (Fig 5). The δD-$\delta^{18}O$ slope surpasses 8 at TX only during winter (DJF), while at BLK only during summer (JJA). In comparison, The δD-$\delta^{18}O$ regression at LL shows slopes all above 8 during the four seasons (Fig. 5a), with autumn particularly demonstrating a slope (8.17) close to the Global Meteorological Water Line (8.2; Rozanski et al. 1992), and a y-intercept (12.89) similar to that for the event-based data in Northeast India (12.34±1.33, Breitenbach et al., 2010) and to the monthly data at Lhasa (12.37; calculated from the GNIP Database accessible at: http://www.iaea.org/water).

The climatic controls over $\delta^{18}O_p$ also exhibit varying seasonality with stations. In the northwestern TP, local control is significant at TX only during winter, when $\delta^{18}O_p$ shows significant negative correlation with precipitation amount (slope: -0.57, R=-0.78, $p<0.05$) (Fig. 5 a, c and d). At BLK, local control is prominent only during autumn, demonstrated by significant temperature effect with a $\delta^{18}O_p$-T slope (0.43‰/℃) falling within the range observed in most continental mid-latitude stations (0.38-0.56‰/℃; Clark and Fritz, 1997; Pearson et al., 1991). The climatic control over $\delta^{18}O_p$ in the southeastern TP is also seasonally sensitive, with autumn as the only season at LL with significant amount effect in this monsoon domain and featuring a $\delta^{18}O_p$-P ratio as -0.06‰/mm (Fig. 5d).

The *d* excess shows significant correlation with $\delta^{18}O_p$ at both BLK and LL during winter (DJF), featuring a significant negative $\delta^{18}O_p$-*d* correlation at BLK (Fig. 5b) whereas a significant positive correlation at LL (Fig. 5a). Such diversity indicates distinct precipitation formation mechanisms at those stations during winter, which will be discussed in the following section.

Despite the different climatic controls in the different seasons at these northwestern TP stations, *d* excess values at TX and BLK in the northwestern TP show similar intra-seasonal variations (Fig. 4a, b), which form a contrast with that at LL in the southeastern TP (Fig. 4c). With *d* excess suggestive of moisture source conditions, the contrast probably indicates distinct atmospheric circulations over the

Atmos. Chem. Phys. Discuss., doi:10.5194/acp-2016-876, 2016
Manuscript under review for journal Atmos. Chem. Phys.
Published: 14 November 2016

Atmospheric Chemistry and Physics Discussions

respective region. To better represent the large-scale atmospheric circulations over such distinct geographical locations, the monthly $\delta^{18}O_p$ and *d*-excess at TX and BLK are composited for the observation period to highlight the common isotopic features in the northwestern TP. Its regional characteristics would form a comparison with those in the southeastern TP. The following discussions for the northwestern TP are based on regional composites.

4. Discussion

4.1 Local versus large scale circulation control over monthly variation of $\delta^{18}O_p$

Isotope-equipped general circulation models offer insight into the isotopic composition of various water bodies in nature, which can help shed light on contributions of different water components to regional precipitation isotopes. To ensure the comparability between model data and observations, we refer to Stable Water Isotope Intercomparison Group, Phase 2 (SWING2) models (Risi et al., 2012) whose outputs contain over three overlapping years with our observation. Output by the nudged LMDZ4 (Laboratoire de Meteorologie Dynamique-Zoom version 4) (Risi et al., 2012) contains monthly data during 2007-2010, and that by the nudged IsoGSM (Yoshimura et al., 2008) contains monthly data during 2007-2009 (Fig. 6). Though both models underestimate the depletion extent of $\delta^{18}O_p$ in the southeastern TP, they simulate the variation amplitude of $\delta^{18}O_p$ in the northwestern TP and the intra-seasonal variation in both regions fairly well (Fig. 6a, b). The correlation coefficients of our observed $\delta^{18}O_p$ with simulations suggest a better performance of the nudged IsoGSM over the southeastern region (Fig. 5a), while a slightly higher sensitivity of the nudged LMDZ4 over the northwestern TP (Fig. 5b).

Besides $\delta^{18}O_p$ in total precipitation, $\delta^{18}O$ in other water bodies in respective models are also available. Similar correlation approach, i.e., least-square linear regression, is therefore applied to analyzing contributions of various water bodies to regional precipitation by comparing and correlating the observed $\delta^{18}O_p$ with isotopic compositions in various water bodies simulated. Those water bodies include, in the IsoGSM, evaporate, river runoff, large-scale and convection precipitation, and total column water vapor (Fig. 6c). In addition, the LMDZ4 model simulation also produces $\delta^{18}O$ in snow, soil and surface flux (Fig. 6d). The $\delta^{18}O$ integrated through the atmospheric water vapor column is regarded as representative of large-scale atmospheric circulation, leaving single-level $\delta^{18}O$ in other water media as representative of local processes (Risi et al., 2010). Least-square linear regression of observed $\delta^{18}O_p$ versus simulated $\delta^{18}O$ in various waters in both models points to significant influence of large-scale atmospheric circulation on $\delta^{18}O_p$ in the monsoon domain, as the most robust correlation is found between water vapor isotopes and $\delta^{18}O_p$ in the southeastern TP (R=0.60, n=43 for the correlation with LMDZ4 simulations; and R=0.56, n=32 with the IsoGSM ones). Similarly, moisture transport at large scales is suggested as the dominant control over monthly $\delta^{18}O_p$ over the northwestern TP, as the best correlation of observed $\delta^{18}O_p$ established by LMDZ4 is with water vapor isotopic composition (R=0.6, n=37). Thus according to the comparatively more genuine model for respective region, the large-scale atmospheric circulation generally dominates the moisture supply to precipitation in both TP regions on a monthly scale.

4.2 Water vapor transport and correlation of $\delta^{18}O_p$ with large-scale atmospheric circulation

The water vapor loaded by the westerly wind split into two branches to the west of the TP in all seasons but summer (Fig. 7). In summer (JJA), the prevailing westerly moisture supply dramatically weakens over the southern TP (Fig. 7 a3 and b3). This is accompanied by a clear intensification of the southwesterly originating from the Indian Ocean (IO), and a noticeable change in the large-scale water vapor transport to the northwestern TP, featured by a significant northward shift of water vapor transport over central Asia and formation of a northwesterly trajectory to the northwestern TP (Fig. 7a3).

The correlation of vertically integrated water vapor flux with $\delta^{18}O_p$ anomalies in the northwestern TP shows seasonally distinct features that are not clearly coincident with the water vapor flux over the region (Fig. 7 a1-4). Winter shows significant positive correlation of $\delta^{18}O_p$ anomalies in the northwestern TP with water vapor along the moisture trajectory, i.e. from the eastern Atlantic, overpassing the Mediterranean Sea and over the northwestern TP. This implies the dominance of westerly over winter precipitation in the region (Fig. 7 a1). In other seasons, $\delta^{18}O_p$ anomalies in the northwest show significant positive correlation with water vapor flux over the equatorial IO and/or the BOB (Fig. 7 a2-4). As contemporary water vapor transport fails to show any southerly supply to the region, this suggests possible tele-connection between the westerly jet and the tropical forcing, which is associated with the northward retreat of the westerly jet with the SASM intensification. With the northward propagation of the SASM influence, the large-scale circulation imposed by the mid-latitude westerly over the northwestern region yields to local evaporation and continental recycling.

The spatial distribution of the correlation map of vertically integrated water vapor divergence with $\delta^{18}O_p$ anomalies over the southeastern TP closely follows the prevailing moisture flux (Fig. 7 b1-4).

Atmos. Chem. Phys. Discuss., doi:10.5194/acp-2016-876, 2016
Manuscript under review for journal Atmos. Chem. Phys.
Published: 14 November 2016

Atmospheric Chemistry and Physics Discussions

The strongly positively correlated area shifts from the southwestern TP during DJF (Fig.7 b1) to the Arabian Sea (AS) during MAM (Fig. 7 b2), which might be associated with the prevalence of mid-latitude westerly during winter while the southward shift of the westerly over and contemporary increase of the oceanic evaporation from the AS during spring. The evolution of the SASM results in shifting of the most closely correlated area from the western region to the equatorial IO during JJA (Fig. 7 b3), and from the far western IO to the nearby central and eastern IO during SON (Fig. 7 b4). The integrated study of correlation map with large-scale atmospheric water vapor flux thus suggests the southeastern TP as mainly supplied by convective precipitation from local processes during DJF and MAM, while by large-scale precipitation from tropical oceans during JJA and SON.

4.3 Isotopic signal of large-scale atmospheric circulation effect

As aforementioned, both the southeastern and northwestern TP are influenced by the southwesterly, which is consistent with the prevalence of the NAM in the mid-latitude in the northern hemisphere. Under the global climate change scenario, changes of the circulation trajectory and intensity associated with NAM evolution affect moisture supply in different parts of the TP, thus likely to leave "footprints" in the isotopic ratio in precipitation in those regions. Moisture borne by the southwesterly originates mainly from the eastern Atlantic and Eurasia for the northwestern TP, while from the tropical oceanic area for the southeastern TP, which explains the general lower *d* excess values in the northwestern TP than the southeastern TP (Table 2), as sub-cloud evaporation is frequent in arid and/or semi-arid environment and decreases *d*-excesses (Froehlich et al., 2008). Besides, studies have confirmed the impacts of ENSO on rainfall in Europe upwind of the northwestern TP (Zanchettin et al., 2008), leaving possible impact of ENSO on the TP inconclusive. Despite the relatively short time span, our data allows a preliminary study of possible ENSO influence on the region, as its sampling period includes 12 months with ENSO warm phase, and 30 months with ENSO cold phase.

Modeling after the division in the ENSO influence study using Niño 3 SST anomalies and a threshold of ± 0.5, the study period is also divided into highly positive (referred to as high NAM)and negative phases (referred to as low NAM) using the AO index and a threshold of ± 1. Study of composites shows distinct meteorological water lines and climatic controls during various NAM and ENSO phases (Table 2). The δD-$\delta^{18}O$ slopes are generally lower in the northwestern (slope<8) than the southeastern TP (slope>8). A δD-$\delta^{18}O$ slope below 8 is usually associated with evaporation during precipitation, which is common for precipitation in the continental semi-arid region (Clark and Fritz,

Atmos. Chem. Phys. Discuss., doi:10.5194/acp-2016-876, 2016
Manuscript under review for journal Atmos. Chem. Phys.
Published: 14 November 2016

1997), as is the case in the northwestern TP. The dramatic decrease of the δD–δ^{18}O slope in the southeastern TP during high NAM period (7.52), likewise, may be attributed to weakening of the precipitation intensity. The decrease in precipitation implies intensifying evaporation during precipitation, resulted in evaporative enrichment and exceptionally high δ^{18}O values in corresponding precipitation during the composite period. Two major atmospheric circulation features associated with the high NAM phase may be responsible for the decrease precipitation and increase evaporation, i.e., 1) intensified westerly jet and 2) weakened meridional wind stream from the south. Feature I implies overlaying of the cold air on top of the comparatively warm air within this subtropical region, considering the mid- and high-tropospheric nature of the mid-latitude westerly. This, on one hand, causes instability of the air in vertical motions, resulting in local convection; while on the other, lowers the cloud condensation height (due to the dominant descent of the cold air), thus minimizing secondary evaporation with the reduced distance between the cloud and ground. Feature II indicates lack of moisture supply form the southern ocean, leading to reduced relative humidity within the region, and thus enhancing the likelihood for evaporation during precipitation. Correspondingly, the isotopic response to these features is the highest d excess value (10.1‰) in the southeastern TP during the high NAM composite of all periods (Table 2), as evaporation increases the d excess (Froehlich et al., 2008). This d value is similar to the global average (10‰; Rozanski et al., 1992; Dansgaard, 1964) that is suggestive of equilibrium fractionation, thereby implying the water vapor as mainly originated from within the region and precipitation formed in a closed cloud system.

Another noticeable composite period is the ENSO warm phase, when the northwestern TP shows dramatic decrease of the *d*-excess (-5.2‰) from its average value (4.2‰), in addition to the significant decrease of both the δD-δ^{18}O slope (7.35) and intercept from the average status (Table 2). This highlights the strong El Nino signal in *d* excess over the northwestern TP, implying potential effect of ENSO on moisture source condition and precipitation status (i.e., evaporation during precipitation and/or precipitation temperature) to the northwestern TP. Also note the simultaneous variation gradient of monthly $\delta^{18}O_p$ with temperature in the northwestern TP, which is small (0.39‰/℃) and constitutes a stark contrast with the gradients during low NAM (0.77‰/℃) or ENSO cold periods (0.72‰/℃). This implies that a 1‰ decrease in monthly $\delta^{18}O_p$ could correspond to a decrease of about 1.3℃ to 2.6℃ in the surface temperature depending on dominant atmospheric circulation pattern, thus highlighting the significance in verifying large-scale atmospheric circulation in temperature reconstruction using $\delta^{18}O_p$.

In comparison, similarity is observed for $\delta^{18}O_p$ in both regions during low NAM and ENSO cold phases, demonstrated by identical δD-$\delta^{18}O_p$ slopes, and lower intercept during the low NAM than the ENSO cold phase (Table 2). The stable variation of the δD- $\delta^{18}O_p$ slopes suggests similarity in atmospheric circulation and precipitation processes during those phases in both TP regions. This has been introduced in a cursory analysis of NAM-related statistics for December and March which suggests analogous structure in the seasonal evolution of the NAM in many respects to the changes observed in association with the ENSO cycle (Quadrelli and Wallace, 2002). Accordingly, the noticeable decrease of the δD-$\delta^{18}O_p$ intercept from Low NAM to ENSO cold phase is believed to be associated with changes at the moisture sources as from warmer (more humid) to cooler (less humid) locations from low NAM to ENSO cold period (Fig 7). This, together with water vapor transport and difference from long-term average, will be discussed in the next section.

Atmos. Chem. Phys. Discuss., doi:10.5194/acp-2016-876, 2016
Manuscript under review for journal Atmos. Chem. Phys.
Published: 14 November 2016

Table 2 Meteorological water lines, amount-weighted $\delta^{18}O_p$ and d-excesses for the northwestern and southeastern TP regions during different composite periods, including high NAM (AO monthly index>1), low NAM (AO monthly index<-1), ENSO cold (Nino3.4 SST anomalies<-0.5) and warm (Nino3.4 SST anomalies >0.5) phases. Correlations surpassing the 0.1 significance level are shown as italics, and those surpassing the 0.05 significance level bolded.

			δD–δ¹⁸O		d excess	$\delta^{18}O_p$ (‰)	δ¹⁸O-T		δ¹⁸O-P	
Location	Climate domain	periods	slope	intercept	(‰)		slope	R	Slope	R
Northwestern TP	Westerly	Average	7.85	-0.64	4.2	-6.5	**0.46**	**0.70**	-0.01	-0.06
		High NAM	7.86	-1.70	3.2	-20.3	**0.51**	**0.77**	-0.03	-0.02
		Low NAM	7.56	-6.74	-1.6	-12.7	**0.77**	**0.61**	-0.06	-0.38
		ENSO Warm	7.35	-10.13	-5.2	-7.1	**0.39**	**0.62**	0.00	0.01
		ENSO cold	7.54	-10.45	-0.5	-2.7	**0.72**	**0.73**	0.56	0.24
Southeastern TP	South Asian summer monsoon	Average	8.34	10.27	6.2	-10.4	**-0.28**	**-0.32**	-0.04	-0.30
		High NAM	7.52	0.22	10.1	-7.9	0.16	0.18	-0.01	-0.04
		Low NAM	8.29	13.40	2.0	-9.4	-0.09	-0.10	-0.07	-0.31
		ENSO Warm	8.59	13.51	4.3	-11.0	*-0.28*	*-0.34*	**-0.05**	**-0.37**
		ENSO cold	8.23	8.13	6.2	-9.0	-0.27	-0.42	-0.02	-0.17

4.4 **Large-scale atmospheric circulation modulates moisture supplies to the southeastern and northwestern TP**

The monthly average status during the past 8 years (Jan 2007-Dec 2014) shows northwestern and southeastern TP as both affected by noticeable water vapor convergence, with a wider coverage and more intensity over the southeastern part (Fig. 8a). This coincides with the much higher humidity in the southeastern than the northwestern TP. The difference of vertically integrated water vapor flux and divergence during selected ENSO and NAM phases from average is more noticeable in the southeastern TP than the northwestern region, suggesting more sensitive response of the southeastern than the northwestern region to ENSO and/or NAM evolutions (Fig 8 b-e).

Over the southeastern TP, water vapor convergence increases during ENSO warm phases, accompanied by intensification of the southwesterly moisture supply (Fig. 8b), and implying convection as water vapor accumulates by pooling oceanic vapor from the south. It diverges during other phases, with the water vapor divergence reaching the maximum during the high NAM period (Fig. 8c-e). Correspondingly, $\delta^{18}O_p$ during ENSO warm phase shows noticeable depletion, both the slope and intercept of the δD- $\delta^{18}O_p$ reaches the highest values, and the amount effect appears significant out of all other composite periods (Table 1). During high NAM phase, otherwise, water vapor strongly diverges over the region, losing moisture to its south. The overwhelming northwesterly moisture supply indicates a transition of the regional climate from a SASM domain to a mid-latitude westerly domain.

The northwestern TP is prevailed by westerly moisture supply in average status (Fig 8a). During ENSO warm phase, there is little change in the water vapor flux and divergence (Fig. 8b), suggesting little effect of the El Niño occurrences on the water vapor availability and transport to the region. During composite periods other than ENSO warm, otherwise, water vapor flux and divergence to its west shows noticeable variation featuring intensified southwesterly moisture supplies and convergence (Fig. 8c-e). The intensification of the southwesterly to the northwestern TP is particularly strong during high NAM (Fig. 8d). This would enhance the water vapor availability to the northwestern TP. Significant cooling of the SST is noticeable in the eastern Atlantic (Fig. 8g), implying low temperature at the moisture source. Both factors thus jointly contribute to the extremely depleted $\delta^{18}O_p$ in the northwestern TP during high NAM (Table 2).

During both the ENSO cold and low NAM phases, otherwise, deviation of the water vapor

Atmos. Chem. Phys. Discuss., doi:10.5194/acp-2016-876, 2016
Manuscript under review for journal Atmos. Chem. Phys.
Published: 14 November 2016

transport from the average status shows increase in water vapor divergence over the southeastern TP (Fig. 8c, e), suggesting the analogous effect of both circulation scenarios on the atmospheric circulation over the region. A detailed investigation reveals slightly weaker increase in divergence and a stronger easterly moisture supply during ENSO cold period (Fig. 8e). Correspondingly, the negative SST anomalies span a wider range during the ENSO cold period than the low NAM period, covering both the mid-latitude eastern Atlantic and the equatorial IO (Fig. 8f, i). The resultant lower temperature at respective moisture source region during ENSO cold period thus might be responsible for a lower δD-$\delta^{18}O$ intercept.

The comparatively stronger roles of high NAM and/or ENSO warm phases to atmospheric circulation over both TP regions can also be appreciated from corresponding SST field and mid-troposphere wind circulation (equivalent to the surface of the TP), as both phases feature distinct patterns from other periods. During the high NAM phase, the SST features strong cooling in the eastern Atlantic to the north of 5° N and in the Mediterranean, while warming in the AS and western equatorial IO (Fig. 8g). The SST contrast thus formed to the immediate south of the TP implies pressure difference, which drives the oceanic water vapor to transport from the south to north. Such a southerly moisture transport, once encountering the prevailing westerly, turns northeastward and contributes to stronger NAM signal than that of tropical forcing in isotopic variation in both regions. Otherwise, the SST during ENSO warm period shows positive anomalies on equal scales in both the northern Atlantic and equatorial IO (Fig. 8h). This could weaken the temperature gradient between the north and south, and slacken the mid-latitude westerly jet, leaving the southeastern TP to SASM dominance and the northwestern TP to local processes.

5 Conclusions

As suggested by output from isotope equipped general circulation models, which perform fairly consistent with our observation data, large-scale atmospheric circulation plays a dominant role in the intra-seasonal variation of $\delta^{18}O_p$ obtained from both the southeastern and northwestern TP.

There are clear but heterogeneous isotopic signals of ENSO and/or NAM involved large-scale atmospheric circulations in both TP regions, highlighting two noteworthy periods for both regions, i.e., the strongly positive NAM and ENSO warm periods. In the northwestern TP, strong positive NAM phase (i.e., high NAM) witnesses extremely low $\delta^{18}O_p$ with little deviation in the slope of the LWML, while ENSO warm phase corresponds to extremely low d-excess, noticeable decrease in δD–$\delta^{18}O$ slope and intercept, and the lowest $\delta^{18}O_p$-T variation ratio of all composite periods. In the southeastern TP, on the other hand, the strongly positive NAM phase corresponds to below-8 a slope and exceptionally low intercept of δD- $\delta^{18}O$ regression, while ENSO warm periods witnesses the highest δD-$\delta^{18}O$ slope and intercept, the lowest $\delta^{18}O_p$ and only significant amount effect of all composite periods.

Water vapor flux and divergence suggest opposite effects of strong positive NAM and/or ENSO warm events on $\delta^{18}O_p$ in the southeastern and northwestern TP. Specifically, ENSO warm phase suppresses the water vapor availability to the northwestern TP, while contributes to the water vapor availability to the southeastern TP. Otherwise, strong positive NAM phase increases the water vapor availability in the northwestern TP by increasing the convergence to the west of the region, while subjects the water vapor transport in the southeastern TP to local processes, thus inducing active evaporation during precipitation over the region. Concomitant variation of SST field and 500 hPa wind demonstrates increasing SST gradient between eastern Atlantic and IO during high NAM, which contributes to the intensification of the large-scale westerly flow. Consequently, the westerly flow overwhelms the SASM in the southeastern TP, which might be responsible for the clearly more depleted $\delta^{18}O_p$. While the weakened temperature contrast between the north and south northern Atlantic Ocean during ENSO warm period slackens the westerly jet, yielding large-scale westerly dominance over the northwestern TP to regional processes, resulting in comparatively more enriched $\delta^{18}O_p$.

Our study offers the first insight into the linkage between the westerly winds and SASM and proposed the potential role of ENSO in modulating the westerly winds and SASM influences over different parts on the TP. More observations and sampling over the Tibetan Plateau are under way and will help better elucidate large-scale atmospheric circulations and their interactions with the TP.

Acknowledgement

This work was supported by the National Natural Science Foundation of China (Grant 41571074), 'Strategic Priority Research Program (B)' of the Chinese Academy of Sciences (Grant No. XDB03030200), CAS Youth Innovation Promotion Association and the China Scholarship Council. The authors acknowledge the efforts of the staff members at the field observation stations for sample collection and recording meteorological data.

References

Aizen, V. B., Aizen, E. M., Joswiak, D. R., Fujita, K., Takeuchi, N., and Nikitin, S. A.: Climatic and atmospheric circulation pattern variability from ice-core isotope/geochemistry records (Altai, Tien Shan and Tibet), Ann Glaciol, 43, 49-60, Doi 10.3189/172756406781812078, 2006.

Allen, R. J., and Zender, C. S.: Forcing of the Arctic Oscillation by Eurasian Snow Cover, J Climate, 24, 6528-6539, 10.1175/2011JCLI4157.1, 2011.

An, Z. S., Colman, S. M., Zhou, W. J., Li, X. Q., Brown, E. T., Jull, A. J. T., Cai, Y. J., Huang, Y. S., Lu, X. F., Chang, H., Song, Y. G., Sun, Y. B., Xu, H., Liu, W. G., Jin, Z. D., Liu, X. D., Cheng, P., Liu, Y., Ai, L., Li, X. Z., Liu, X. J., Yan, L. B., Shi, Z. G., Wang, X. L., Wu, F., Qiang, X. K., Dong, J. B., Lu, F. Y., and Xu, X. W.: Interplay between the Westerlies and Asian monsoon recorded in Lake Qinghai sediments since 32 ka, Sci Rep-Uk, 2, Artn 61910.1038/Srep00619, 2012.

Araguas-Araguas, L., Froehlich, K., and Rozanski, K.: Deuterium and oxygen-18 isotope composition of precipitation and atmospheric moisture, Hydrol Process, 14, 1341-1355, Doi 10.1002/1099-1085(20000615)14:8<1341::Aid-Hyp983>3.0.Co;2-Z, 2000.

Bamzai, A. S., and Shukla, J.: Relation between Eurasian snow cover, snow depth, and the Indian summer monsoon: An observational study, J Climate, 12, 3117-3132, Doi 10.1175/1520-0442(1999)012<3117:Rbescs>2.0.Co;2, 1999.

Bolch, T., Kulkarni, A., Kaab, A., Huggel, C., Paul, F., Cogley, J. G., Frey, H., Kargel, J. S., Fujita, K., Scheel, M., Bajracharya, S., and Stoffel, M.: The State and Fate of Himalayan Glaciers, Science, 336, 310-314, 10.1126/science.1215828, 2012.

Chiang, J. C. H., Fung, I. Y., Wu, C. H., Cai, Y. H., Edman, J. P., Liu, Y. W., Day, J. A., Bhattacharya, T., Mondal, Y., and Labrousse, C. A.: Role of seasonal transitions and westerly jets in East Asian paleoclimate, Quaternary Sci Rev, 108, 111-129, 10.1016/j.quascirev.2014.11.009, 2015.

Clark, I., and Fritz, P.: Environmental isotopes in Hydrogeology, Lewis Publishers, United States of America, 1997.

Conroy, J. L., and Overpeck, J. T.: Regionalization of Present-Day Precipitation in the Greater Monsoon Region of Asia, J Climate, 24, 4073-4095, 10.1175/2011JCLI4033.1, 2011.

Dansgaard, W.: Stable Isotopes in Precipitation, Tellus, 16, 436-468, 1964.

Ding, Q. H., Wallace, J. M., Battisti, D. S., Steig, E. J., Gallant, A. J. E., Kim, H. J., and Geng, L.: Tropical forcing of the recent rapid Arctic warming in northeastern Canada and Greenland, Nature, 509, 209-+, 10.1038/nature13260, 2014.

Froehlich, K., Kralik, M., Papesch, W., Rank, D., Scheifinger, H., and Stichler, W.: Deuterium excess in precipitation of Alpine regions - moisture recycling, Isot Environ Healt S, 44, 61-70, 10.1080/10256010801887208, 2008.

Fujita, K.: Effect of precipitation seasonality on climatic sensitivity of glacier mass balance, Earth Planet Sc Lett, 276, 14-19, 10.1016/j.epsl.2008.08.028, 2008.

Gardner, A. S., Moholdt, G., Cogley, J. G., Wouters, B., Arendt, A. A., Wahr, J., Berthier, E., Hock, R., Pfeffer, W. T., Kaser, G., Ligtenberg, S. R. M., Bolch, T., Sharp, M. J., Hagen, J. O., van den Broeke, M. R., and Paul, F.: A Reconciled Estimate of Glacier Contributions to Sea Level Rise: 2003 to 2009,

Atmos. Chem. Phys. Discuss., doi:10.5194/acp-2016-876, 2016
Manuscript under review for journal Atmos. Chem. Phys.
Published: 14 November 2016

Atmospheric Chemistry and Physics Discussions

Science, 340, 852-857, 10.1126/science.1234532, 2013.

Immerzeel, W. W., and Bierkens, M. F. P.: Asian Water Towers: More on Monsoons Response, Science, 330, 585-585, 2010.

Kendall, C., and Caldwell, E. A.: Fundamentals of isotope geochemistry, in: Isotope Tracers in Catchment Hydrology, edited by: Kendall, C., and McDonnell, J. J., Elsevier Science B. V., Amsterdam, 51-86, 1998.

Liu, X. D., and Yin, Z. Y.: Spatial and temporal variation of summer precipitation over the eastern Tibetan Plateau and the North Atlantic oscillation, J Climate, 14, 2896-2909, Doi 10.1175/1520-0442(2001)014<2896:Satvos>2.0.Co;2, 2001.

Lu, J. M., Ju, J. H., Kim, S. J., Ren, J. Z., and Zhu, Y. X.: Arctic Oscillation and the autumn/winter snow depth over the Tibetan Plateau, J Geophys Res-Atmos, 113, Artn D14117, doi: 10.1029/2007jd009567, 2008.

Park, H. S., Chiang, J. C. H., and Bordoni, S.: The Mechanical Impact of the Tibetan Plateau on the Seasonal Evolution of the South Asian Monsoon, J Climate, 25, 2394-2407, 10.1175/Jcli-D-11-00281.1, 2012.

Pearson, D. G., Davies, G. R., Nixon, P. H., Greenwood, P. B., and Mattey, D. P.: Oxygen Isotope Evidence for the Origin of Pyroxenites in the Beni Bousera Peridotite Massif, North Morocco - Derivation from Subducted Oceanic Lithosphere, Earth Planet Sc Lett, 102, 289-301, Doi 10.1016/0012-821x(91)90024-C, 1991.

Quadrelli, R., and Wallace, J. M.: Dependence of the structure of the Northern Hemisphere annular mode on the polarity of ENSO, Geophys Res Lett, 29, Artn 2132, doi: 10.1029/2002gl015807, 2002.

Rayner, N. A., Parker, D. E., Horton, E. B., Folland, C. K., Alexander, L. V., Rowell, D. P., Kent, E. C., and Kaplan, A.: Global analyses of sea surface temperature, sea ice, and night marine air temperature since the late nineteenth century, J Geophys Res-Atmos, 108, 10.1029/2002jd002670, 2003.

Risi, C., Noone, D., Worden, J., Frankenberg, C., Stiller, G., Kiefer, M., Funke, B., Walker, K., Bernath, P., Schneider, M., Bony, S., Lee, J., Brown, D., and Sturm, C.: Process-evaluation of tropospheric humidity simulated by general circulation models using water vapor isotopic observations: 2. Using isotopic diagnostics to understand the mid and upper tropospheric moist bias in the tropics and subtropics, J Geophys Res-Atmos, 117, Artn D05304, 10.1029/2011jd016623, 2012.

Rowley, D. B., and Garzione, C. N.: Stable isotope-based paleoaltimetry, Annual Review of Earth and Planetary Sciences, 35, 463-508, 10.1146/annurev.earth.35.031306.140155, 2007.

Rozanski, K., Araguasaraguas, L., and Gonfiantini, R.: Relation between Long-Term Trends of O-18 Isotope Composition of Precipitation and Climate, Science, 258, 981-985, DOI 10.1126/science.258.5084.981, 1992.

Sugimoto, S., and Ueno, K.: Formation of mesoscale convective systems over the eastern Tibetan Plateau affected by plateau-scale heating contrasts, J Geophys Res-Atmos, 115, Artn D16105, 10.1029/2009jd013609, 2010.

Thompson, L. G., Mosley-Thompson, E., Davis, M. E., and Brecher, H. H.: Tropical glaciers, recorders and indicators of climate change, are disappearing globally, Annals of Glaciology, 52, 23-34, 2011.

Tian, L. D., Yao, T. D., MacClune, K., White, J. W. C., Schilla, A., Vaughn, B., Vachon, R., and Ichiyanagi, K.: Stable isotopic variations in west China: A consideration of moisture sources, J Geophys Res-Atmos, 112, Artn D10112, 10.1029/2006jd007718, 2007.

Vuille, M., Werner, M., Bradley, R. S., and Keimig, F.: Stable isotopes in precipitation in the Asian monsoon region, J Geophys Res-Atmos, 110, Artn D23108, 10.1029/2005jd006022, 2005.

Wu, G. X., and Zhang, Y. S.: Tibetan Plateau forcing and the timing of the monsoon onset over South Asia and the South China Sea, Mon Weather Rev, 126, 913-927, Doi 10.1175/1520-0493(1998)126<0913:Tpfatt>2.0.Co;2, 1998.

Xu, B. Q., Wang, M., Joswiak, D. R., Cao, J. J., Yao, T. D., Wu, G. J., Yang, W., and Zhao, H. B.: Deposition of anthropogenic aerosols in a southeastern Tibetan glacier, J Geophys Res-Atmos, 114, Artn D17209, 10.1029/2008jd011510, 2009.

Yang, X. X., Yao, T. D., Yang, W. L., Xu, B. Q., He, Y., and Qu, D. M.: Isotopic Signal of Earlier Summer Monsoon Onset in the Bay of Bengal, J Climate, 25, 2509-2516, 10.1175/Jcli-D-11-00180.1, 2012.

Yao, T. D., Thompson, L., Yang, W., Yu, W. S., Gao, Y., Guo, X. J., Yang, X. X., Duan, K. Q., Zhao, H. B., Xu, B. Q., Pu, J. C., Lu, A. X., Xiang, Y., Kattel, D. B., and Joswiak, D.: Different glacier status with atmospheric circulations in Tibetan Plateau and surroundings, Nat Clim Change, 2, 663-667, 10.1038/Nclimate1580, 2012.

Yao, T. D., Masson-Delmotte, V., Gao, J., Yu, W. S., Yang, X. X., Risi, C., Sturm, C., Werner, M., Zhao, H. B., He, Y., Ren, W., Tian, L. D., Shi, C. M., and Hou, S. G.: A review of climatic controls on delta O-18 in precipitation over the Tibetan Plateau: observations and simulations, Rev Geophys, 51, Artn

2012rg000427, doi: 10.1002/Rog.20023, 2013.
Ye, D. Z., and Wu, G. X.: The role of the heat source of the Tibetan Plateau in the general circulation, Meteorol Atmos Phys, 67, 181-198, Doi 10.1007/Bf01277509, 1998.
Yoshimura, K., Kanamitsu, M., Noone, D., and Oki, T.: Historical isotope simulation using Reanalysis atmospheric data, J Geophys Res-Atmos, 113, Artn D19108, 10.1029/2008jd010074, 2008.
Zanchettin, D., Franks, S. W., Traverso, P., and Tomasino, M.: On ENSO impacts on European wintertime rainfalls and their modulation by the NAO and the Pacific multi-decadal variability described through the PDO index, Int J Climatol, 28, 995-1006, 10.1002/joc.1601, 2008.
Zhao, P., Zhou, Z. J., and Liu, J. P.: Variability of Tibetan spring snow and its associations with the hemispheric extratropical circulation and East Asian summer monsoon rainfall: An observational investigation, J Climate, 20, 3942-3955, 10.1175/JCLI4205.1, 2007.
Zhao, Y., Huang, A. N., Zhou, Y., Huang, D. Q., Yang, Q., Ma, Y. F., Li, M., and Wei, G.: Impact of the Middle and Upper Tropospheric Cooling over Central Asia on the Summer Rainfall in the Tarim Basin, China, J Climate, 27, 4721-4732, 10.1175/Jcli-D-13-00456.1, 2014.

Atmos. Chem. Phys. Discuss., doi:10.5194/acp-2016-876, 2016
Manuscript under review for journal Atmos. Chem. Phys.
Published: 14 November 2016

Figure files

Figure Captions:

Figure 1 Spatial distribution of $\delta^{18}O_p$ based on GNIP, superimposed on the long-term climatological wind circulation in January (upper) and July (lower). The climatological isotope map is adapted from www-naweb.iaea.org/napc/ih/documents/user-update/waterloo/index.html, with 'weighted $\delta^{18}O_p$' meaning $\delta^{18}O_p$ values weighted by precipitation amount. The wind circulation is plotted from the long-term mean zonal and meridional wind (1981-2010) from the NCEP/NCAR reanalysis.

Figure 2 Location of our sampling sites (black triangles) on a digital elevation map (DEM). Also shown are reference sites (black dots) mentioned in this study. Colored map on the lower left corner depicts the detailed topographic status over the northwestern TP. The DEM is based on Processed SRTM Data v4.1, which are derived from the USGS/NASA SRTM data, but are processed to provide seamless continuous topography surfaces.

Figure 3 Monthly and long-term seasonality of $\delta^{18}O_p$ (black dots), temperature (red dots), and precipitation (vertical bar), together with monthly d excess (open dots) in (a) and (d) TX, (b) and (e) BLK and (c) and (f) LL. Climatology and error bars for long-term seasonal $\delta^{18}O_p$ means are calculated from available data record during covered periods shown in Table 1.

Figure 4 Box-whisker plot of monthly d excesses at the three stations: (a) TX, (b) BLK and (c) LL. On each box, the central mark is the median, the edges of the box are the 25th and 75th percentiles, the whiskers extend to the most extreme data points the algorithm considers to be not outliers, and the outliers are plotted individually.

Figure 5 Seasonality of slopes and intercepts of the linear correlations for (a) monthly δD-$\delta^{18}O$, (b) monthly $\delta^{18}O$-d excess, (c) monthly $\delta^{18}O$-T, and (d) monthly $\delta^{18}O$-P. Blue dots in (b)-(d) highlight those correlations significant at 0.05 confidence level.

Atmos. Chem. Phys. Discuss., doi:10.5194/acp-2016-876, 2016
Manuscript under review for journal Atmos. Chem. Phys.
Published: 14 November 2016

Atmospheric Chemistry and Physics Discussions
Open Access

Figure 6 Comparison of time-series variation of observed $\delta^{18}O_p$ with $\delta^{18}O$ in various water bodies simulated by models in SWING2. (a) comparison of observed versus modeled $\delta^{18}O_p$ for the southeastern TP; (b) same as (a), but for the northwestern TP; (c) comparison of observed $\delta^{18}O_p$ in the southeastern (upper) and northwestern (lower) TP versus $\delta^{18}O$ in various water bodies simulated by nudged IsoGSM; (d) same as (c), but with $\delta^{18}O$ in various water bodies simulated by nudged LMDZ4. Variation ratios explainable by simulated $\delta^{18}O_p$ are listed in the upright corner in (a) and (b). $\delta^{18}O_p$ integral in the atmospheric water vapor column is used to represent large-scale atmospheric transport. Full names for abbreviations used in (c) and (d) are listed as follows: O_ob: $\delta^{18}O$ of our station data, wv: water vapor $\delta^{18}O$, evp: evaporation $\delta^{18}O$, CP: $\delta^{18}O$ in convective precipitation, LP: $\delta^{18}O$ in large-scale precipitation, and surfx: $\delta^{18}O$ in surface flux.

Figure 7 Water vapor transport and spatial correlation map of monthly $\delta^{18}O_p$ anomalies with vertically integrated water vapor flux for December-February (DJF) (a1, b1), March-May (MAM) (a2, b2), June-August (JJA) (a3, b3) and September-November (SON) (a4, b4). Among them, a1-4 are fore the correlation for the northwestern TP, while b1-4 for the southeastern TP. Correlations exceeding the 0.1 significance level are shown (red/positive; blue/negative). "nw" and "se" in the upper left of each panel refer to, respectively, northwestern and southeastern TP. "Oa" means $\delta^{18}O_p$ anomalies calculated as the difference between monthly $\delta^{18}O_p$ and 8-year monthly mean values. Vertically integrated water vapor flux and divergence are downloaded from ERA-interim reanalysis data.

Figure 8 (a)-(e) average status of water vapor transport and flux, and difference between different periodical composite and the average status: (a) average status of water vapor flux and transport to the TP, (b) difference between ENSO warm period and the average; (c) difference between ENSO cold period and the average, (d) difference between high NAM period and the average, and (e) difference between low NAM period and the average. Vertical integral of water vapor flux (shaded) and divergence (vector) are plotted from ERA-interim monthly reanalysis data. (f)-(i) SST anomalies and 500 hPa wind circulation composited for: (f) low NAM, (g) high NAM, (h) ENSO warm, and (i) ENSO cold periods. SST data are from HadISST monthly data. Anomalies are calculated with 1981-2010 as the base period. Zonal and meridional wind is from ERA-interim reanalysis dataset.

Atmos. Chem. Phys. Discuss., doi:10.5194/acp-2016-876, 2016
Manuscript under review for journal Atmos. Chem. Phys.
Published: 14 November 2016

Figure 1

Weighted Jan. $\delta^{18}O$

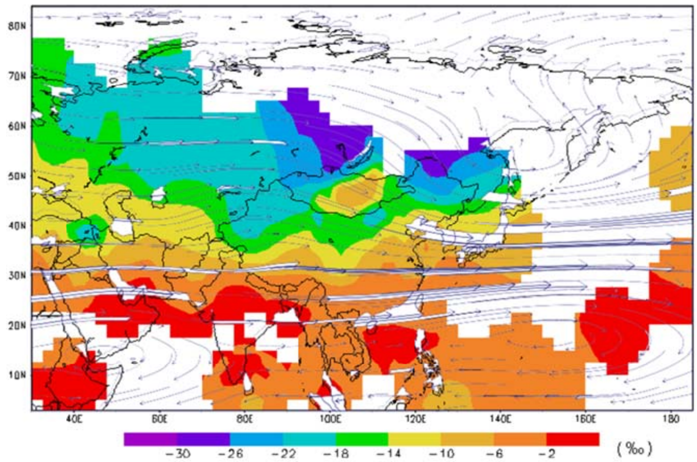

Weighted July $\delta^{18}O$

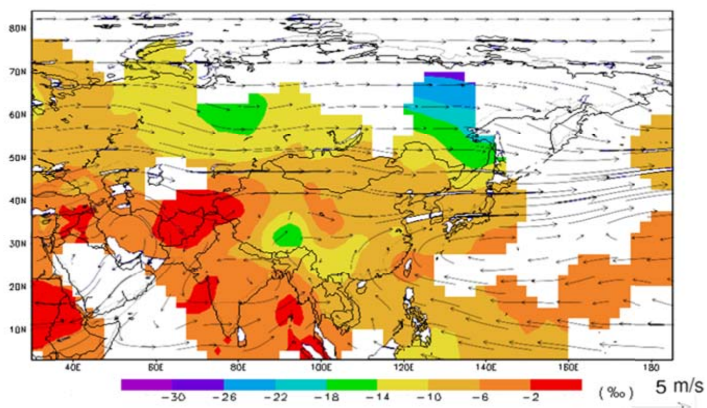

Atmos. Chem. Phys. Discuss., doi:10.5194/acp-2016-876, 2016
Manuscript under review for journal Atmos. Chem. Phys.
Published: 14 November 2016

Atmospheric Chemistry and Physics
Discussions
Open Access

Figure 2

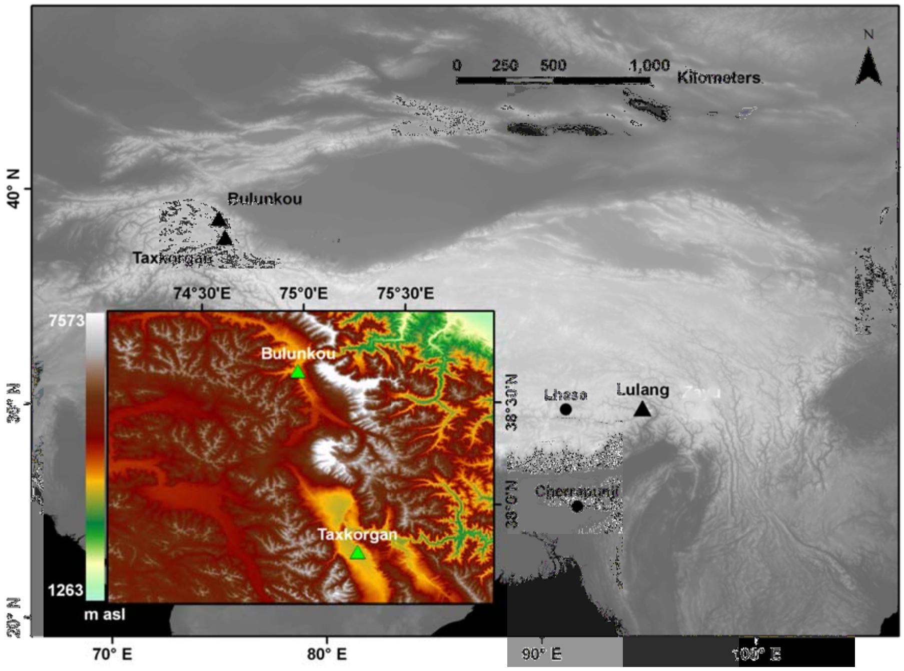

Atmos. Chem. Phys. Discuss., doi:10.5194/acp-2016-876, 2016
Manuscript under review for journal Atmos. Chem. Phys.
Published: 14 November 2016

Figure 3

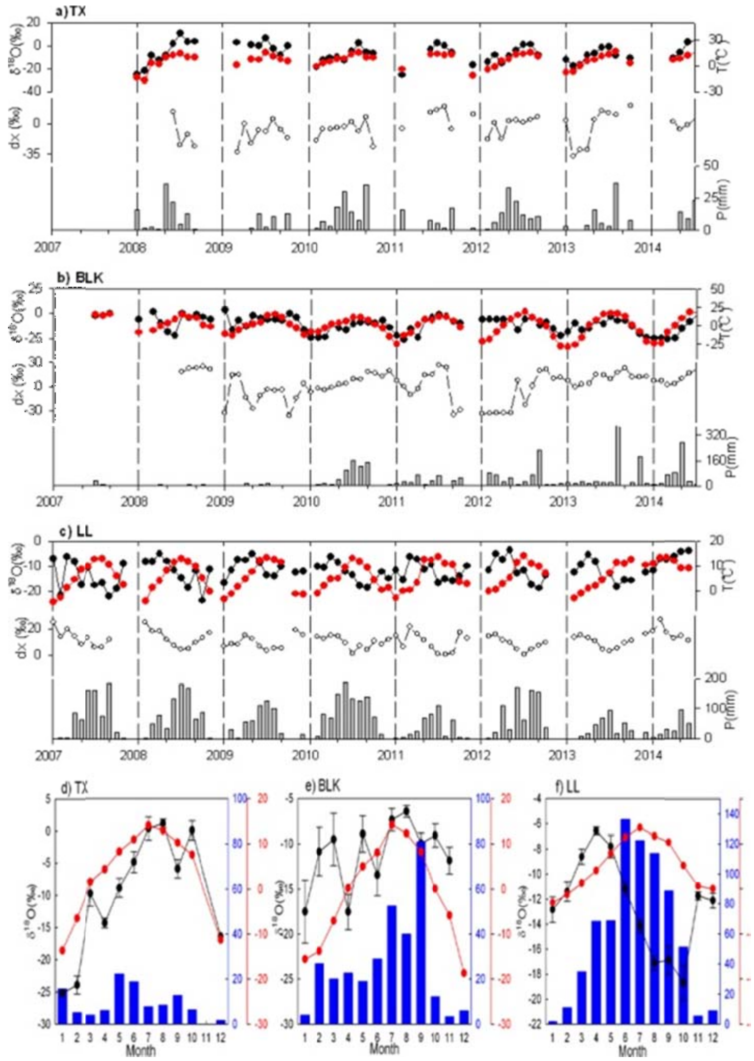

Atmos. Chem. Phys. Discuss., doi:10.5194/acp-2016-876, 2016
Manuscript under review for journal Atmos. Chem. Phys.
Published: 14 November 2016

Figure 4

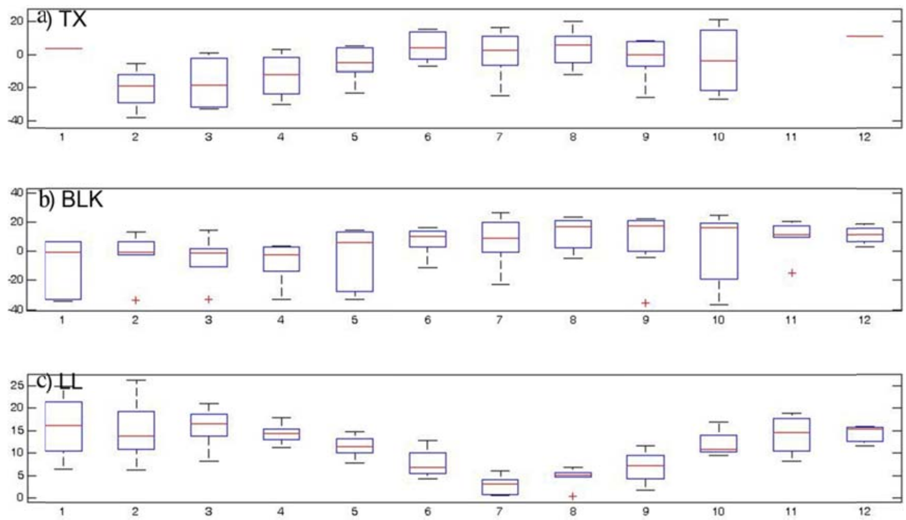

Atmos. Chem. Phys. Discuss., doi:10.5194/acp-2016-876, 2016
Manuscript under review for journal Atmos. Chem. Phys.
Published: 14 November 2016

Atmospheric Chemistry and Physics
Discussions

Figure 5

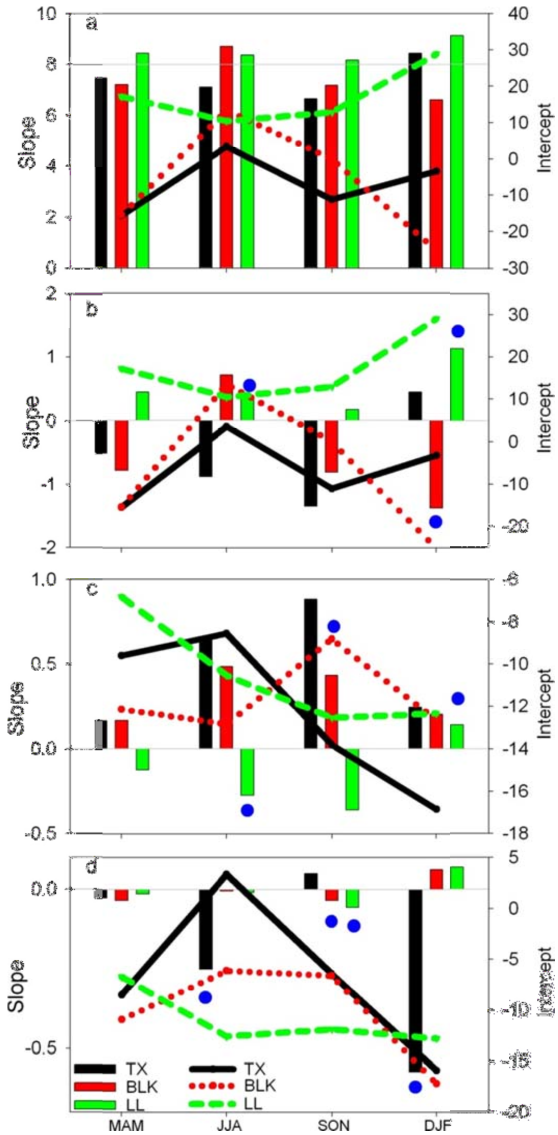

Atmos. Chem. Phys. Discuss., doi:10.5194/acp-2016-876, 2016
Manuscript under review for journal Atmos. Chem. Phys.
Published: 14 November 2016

Figure 6

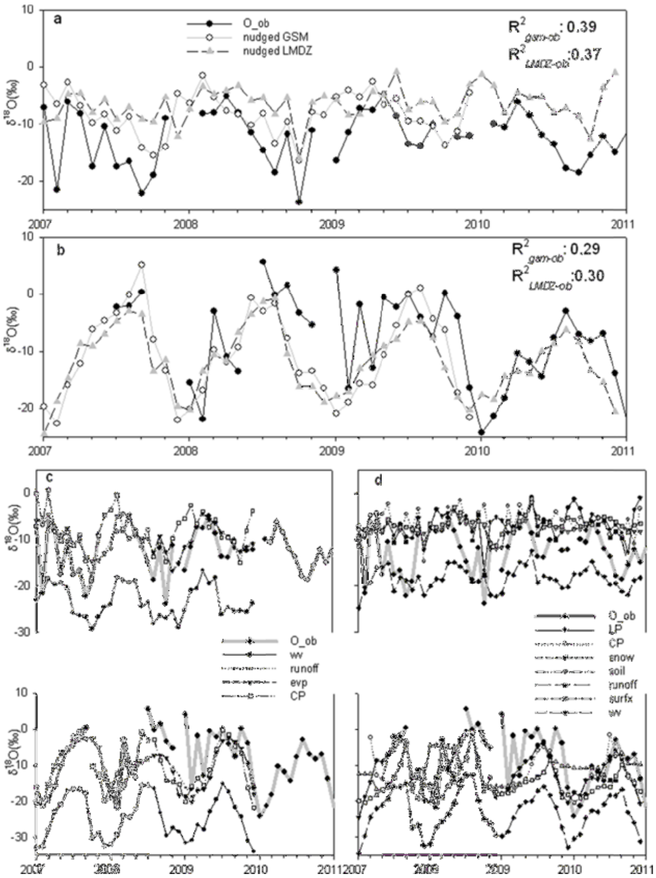

Atmos. Chem. Phys. Discuss., doi:10.5194/acp-2016-876, 2016
Manuscript under review for journal Atmos. Chem. Phys.
Published: 14 November 2016

Atmospheric Chemistry and Physics
Discussions
Open Access

Figure 7

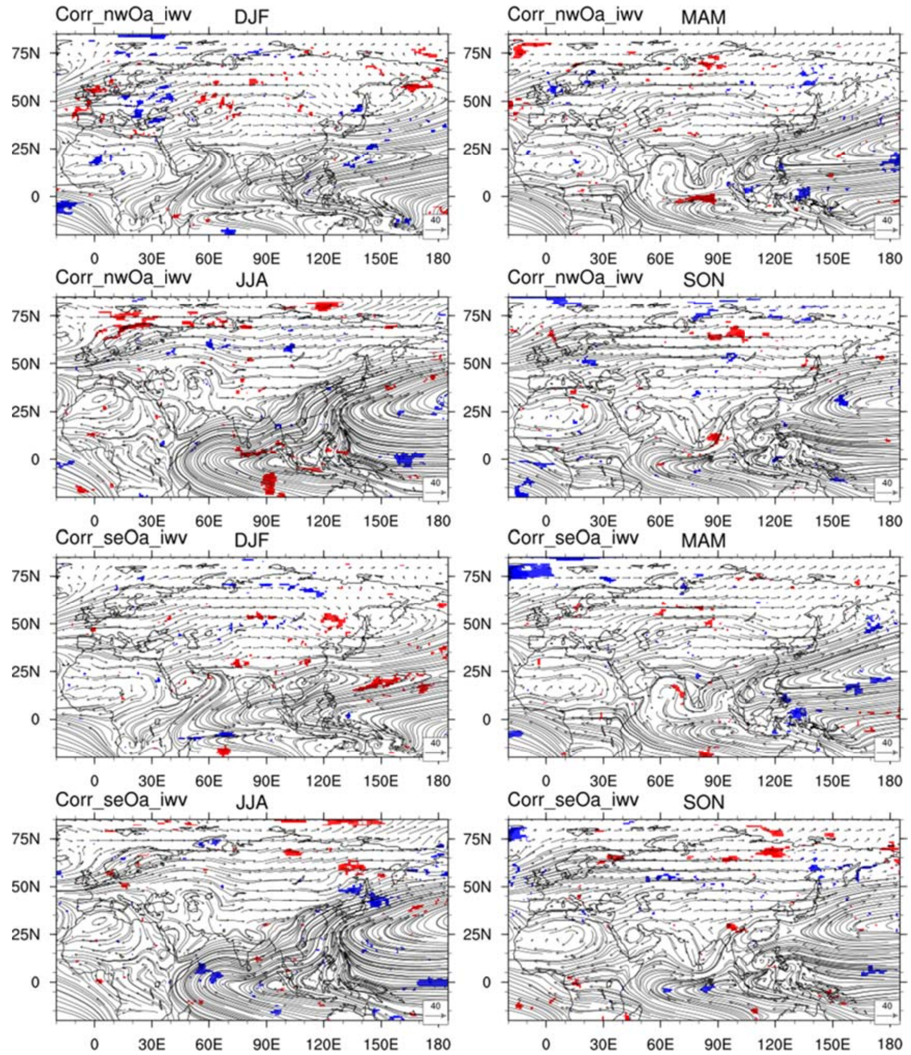

Atmos. Chem. Phys. Discuss., doi:10.5194/acp-2016-876, 2016
Manuscript under review for journal Atmos. Chem. Phys.
Published: 14 November 2016

Figure 8